Texture Evolution in Mg-Zn-Ca Alloy Sheets

D.-W. KIM, B.-C. SUH, M.-S. SHIM, J.H. BAE, D.H. KIM, and NACK J. KIM

Ca was added to Mg-1Zn and Mg-6Zn alloys to modify their texture, and the origin of texture modification by Ca addition has been investigated. It shows that Mg-1Zn-1Ca (ZX11) and Mg-6Zn-1Ca (ZX61) alloy sheets in the as-rolled condition show the textures having a splitting of basal poles toward the rolling direction and a splitting of basal poles toward the transverse direction, respectively. An analysis of the microstructure in the as-rolled condition shows that two different types of twins become active during rolling, double twins for ZX11 and tension twins for ZX61, suggesting that double twinning and tension twinning promote a splitting of basal poles toward the rolling direction (ZX11) and transverse direction (ZX61), respectively. On the other hand, after annealing, both alloy sheets show a weakened texture characterized by a splitting of basal poles toward the transverse direction. During annealing, the growth of tension twin-oriented grains occurs, resulting in the texture having a splitting of basal poles toward the transverse direction in both alloys. These alloys show not only higher yield strength but also better stretch formability than Al 5052 alloy, showing their potential as highly formable Mg sheet alloys.

DOI: 10.1007/s11661-013-1674-2

I. INTRODUCTION

IT is well known that Mg alloy sheets exhibit strong basal textures after thermomechanical treatment. Such a strong basal texture of Mg alloy sheets has an adverse effect on ductility and formability at room temperature. It has been demonstrated in several studies that the weakening of texture significantly improves the formability of Mg alloy sheets at room temperature.[1–4] Therefore, there have been numerous studies[5–16] on modifying the texture of Mg alloy sheets to a weaker and more random distribution of basal poles. It has been shown that the addition of rare earth (RE) elements such as Ce, Nd, and Y, for example, can significantly weaken and randomize the texture of Mg alloy sheets.[10–16] The texture of these alloy sheets is typically characterized by the broadening of angular distribution of basal poles along the transverse direction (TD). However, their peak positions vary among the alloys. Some alloy sheets show the splitting of the maximum basal pole intensity along the rolling direction (RD),[10–13] while others show it along the TD.[14–16] Despite such a beneficial effect of RE elements on the modification of texture in warm- or hot-rolled Mg alloys, the high costs of these elements might prevent their widespread utilization as alloying elements for wrought Mg alloys. Therefore, it is necessary to find alternative alloying elements which have similar effects on texture evolution to those of RE elements. It has been recently shown that some of the Ca-containing alloys have weaker and more random textures[4,17,18] and better formability[4,19] than the ones without Ca addition. However, the detailed mechanisms responsible for such texture modifications by the addition of Ca are not clearly understood yet. In the present study, the effect of Ca addition on texture evolution and mechanical properties of Mg-Zn base alloys has been investigated.

II. EXPERIMENTAL PROCEDURE

Alloys with nominal compositions of Mg-1Zn-1Ca (ZX11) and Mg-6Zn-1Ca (ZX61) in wt pct were prepared by induction melting using a steel crucible under Ar atmosphere. Analyzed compositions are Mg-0.95Zn-0.9Ca and Mg-5.99Zn-0.98Ca for ZX11 and ZX61, respectively. The alloys were remelted under an inert atmosphere of CO_2 and SF_6 mixture and the molten alloys were transferred into preheated tundish the temperature of which was set at 983 K (710 °C), followed by twin-roll casting (TRC). The roll gap was set at 1.8 mm and roll speed was 4 m/min. Details of the TRC process are described elsewhere.[20–22] Cast alloys were subsequently thermomechanically treated. They were homogenized at 713 K (440 °C) for 1 h for ZX11 and at 623 K (350 °C) for 1 h for ZX61, followed by water quenching. Homogenizing temperatures were selected based on the results of differential scanning calorimetry (DSC) to prevent the occurrence of incipient

D.-W. KIM, B.-C. SUH, and M.-S. SHIM, Graduate Students, are with the Center for Advanced Aerospace Materials, Pohang University of Science and Technology (POSTECH), Pohang 790-784, South Korea, and also with the Department of Materials Science and Engineering, Pohang University of Science and Technology (POSTECH). J.H. BAE, Senior Researcher, is with the Korea Institute of Materials Science, Changwon 641-831, South Korea. D.H. KIM, Professor, is with the Center for Non-crystalline Materials, Yonsei University, Seoul, South Korea. NACK J. KIM, Professor, is with the Center for Advanced Aerospace Materials, Pohang University of Science and Technology (POSTECH), and also with the Graduate Institute of Ferrous Technology, Pohang University of Science and Technology (POSTECH). Contact e-mail: njkim@postech.ac.kr
Manuscript submitted June 11, 2012.
Article published online March 2, 2013

melting. The homogenized alloys were hot rolled at 573 K (300 °C) for 5 passes with a total reduction of 50 pct (13 pct reduction per pass). After each rolling pass, the sheet was reheated at 573 K (300 °C) for 20 minutes prior to subsequent rolling. After the final rolling, the sheets were given a final annealing treatment at 713 K (440 °C) for 30 minutes for ZX11 and at 623 K (350 °C) for 30 minutes for ZX61, followed by water quenching (T4). Optical microscopy, electron back-scattered diffraction (EBSD), and transmission electron microscopy (TEM) were conducted on cross sections perpendicular to the TD of the sheets.

EBSD analyses were conducted using a Quanta 3D FEG SEM equipped with a TSL EBSD system. Imaging of crystal orientation using EBSD involved automatic beam scanning with a step size of 0.2 to 0.3 μm, map size of 100 × 300 μm, and indexing rate of ~250 points/second. Orientation imaging microscopy (OIM) Analysis 5.2 software was used to analyze the EBSD measurement results. OIM maps were subject to two clean-up algorithm procedures. Imposing a confidence index (CI) value (*e.g.*, CI >0.1) was required to filter points with bad quality patterns or uncertain indexing. For the clean-up, neighbor orientation correlation was applied with a grain tolerance angle of 5 deg, minimum confidence of 0, clean-up level of 5, and minimum grain size of 5 pixels.

Thin foil specimens for TEM were prepared by punching 3-mm-diameter disks and twin jet electropolishing in a solution of 60 vol pct methanol, 30 vol pct nitric acid, and 10 vol pct glycerol at 25 V and then by ion beam milling. The crystallographic texture of the alloys after each rolling step was analyzed on the midsection of the specimens using Mo K_α radiation at 3 kW with a measuring grid of 5 deg × 5 deg in both polar and azimuthal rotations of the specimen to a maximum tilt of 70 deg. Pole figures were obtained from five different planes, (10.0), (00.2), (10.1), (10.2), and (10.3), using the Schulz reflection method, and these pole figures were recalculated back from the ODF and were normalized to correct the defocusing effect. The XRD data were processed using TexTool v. 3.3 software.

Tensile properties were measured using flat tensile specimens with 12.6 mm gage length, 1 mm gage thickness, and 5 mm gage width. The strain rate used was 6.4×10^{-4} s^{-1}. Stretch formability was evaluated by the limiting dome height (LDH) value obtained by the Erichsen cupping test (disk-shaped specimen with 50 mm diameter). The punch diameter and speed used were 27.5 mm and 0.1 mm s^{-1}, respectively. Silicon oil was used as a lubricant. Thermodynamic calculations of the phase evolution were conducted using FactSage 6.2.

III. RESULTS

A. *Microstructure*

The microstructures of the alloy sheets in various conditions are shown in Figures 1 and 2. In the as-cast condition, both alloys show a typical cast structure consisting of dendritic columnar grains (Figures 1(a) and 1(b)). After homogenization, ZX11 shows an equiaxed grain structure (Figure 2(a)), while ZX 61 still shows a dendritic columnar grain structure resembling that of the as-cast structure (Figure 2(f)). Such a difference in the as-homogenized microstructure is possibly due to the difference in homogenization temperatures [713 K and 623 K (440 °C and 350 °C) for ZX11 and ZX61, respectively], which were chosen to homogenize the alloy without the occurrence of incipient melting. After the first rolling pass (Figure 2(b)) of ZX11, there is a formation of deformation bands (for example, see the circled area in Figure 2(b)), which have specific orientations within the grain and therefore change the direction across the grains. In the sheet rolled three times (Figure 2(c)), the microstructure consists of the grains partially elongated, which persists up to the fourth rolling pass. The microstructure becomes finer and partially equiaxed after the final fifth rolling pass (Figure 2(d)). It is after the final annealing that the grain structure becomes a fully recrystallized structure with an average grain size of ~7.7 μm (Figure 2(e)), which is larger than the average grain size (~4.3 μm) of the sheet rolled five times. As is the case of ZX11, there is virtually no change in the grain structure of ZX61 after the first rolling pass, except the formation of deformation bands (for example, see the circled area in Figure 2(g)). After the second rolling pass, the grain structure becomes

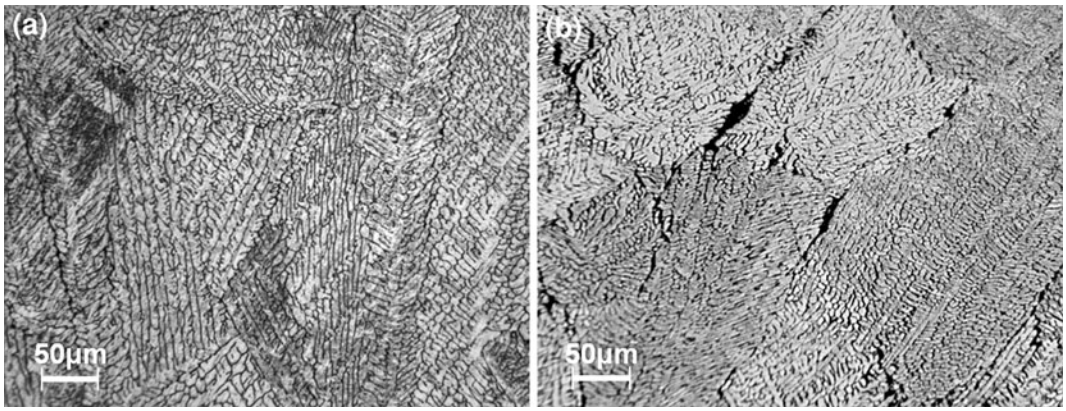

Fig. 1—Optical micrographs of the alloys in the as-cast condition; (*a*) ZX11 and (*b*) ZX61.

distinct with a large amount of twins [for example, see the circled area in Figure 2(h)]. Such a microstructure persists up to the final fifth rolling pass (Figure 2(i)). After the final annealing, grains becomes fully recrystallized with an average grain size of ~7.4 μm (Figure 2(j)), which is quite similar to that of ZX11.

As can be seen in the optical micrographs of Figures 2(a) through (j), there are second-phase particles in both ZX11 and ZX61. They are present with various morphologies: within the matrix, along grain boundaries, and in stringer forms. TEM analyses have been conducted to identify the nature of the second-phase particles. It shows that the second phases in ZX11 and ZX61 are mostly Mg_2Ca (Figures 3(a)) and $Mg_6Zn_3Ca_2$ (Figure 3(b)), respectively. The calculation of the volume fractions of the second-phase particles by the image analyses shows that ZX11 has a smaller amount of second-phase particles than ZX61 (1.9 *vs* 5.8 pct).

Typical EBSD inverse pole figure (IPF) maps of one-pass-rolled specimens are shown in Figure 4. It shows that ZX11 alloy contains both {10.1}{10.2} double twins and {10.2} tension twins (Figure 4(a)), while ZX61 alloy contains mostly tension twins (Figure 4(b)). Distribution of the boundary misorientation angle also confirms the presence of both double twins (at around 38 deg) and tension twins (86 deg) in ZX11 alloy and tension twins in ZX61 alloy. Since the alloys show a large difference in twinning behavior during rolling, variations in the boundary misorientation of the alloys with rolling have been determined from EBSD data as shown in Figure 5. It shows that in the as-homogenized condition, ZX11 has a random distribution of misorientation angles. After the first rolling pass, there are large fractions near the misorientation angles of 38 and 86 deg as previously mentioned, indicating that there are formations of {10.1}{10.2} double twins and {10.2} tension twins, respectively. The fractions near the misorientation angles of 38 and 86 deg related with double twins and tension twins diminish with increasing the number of rolling passes. Although the fractions of

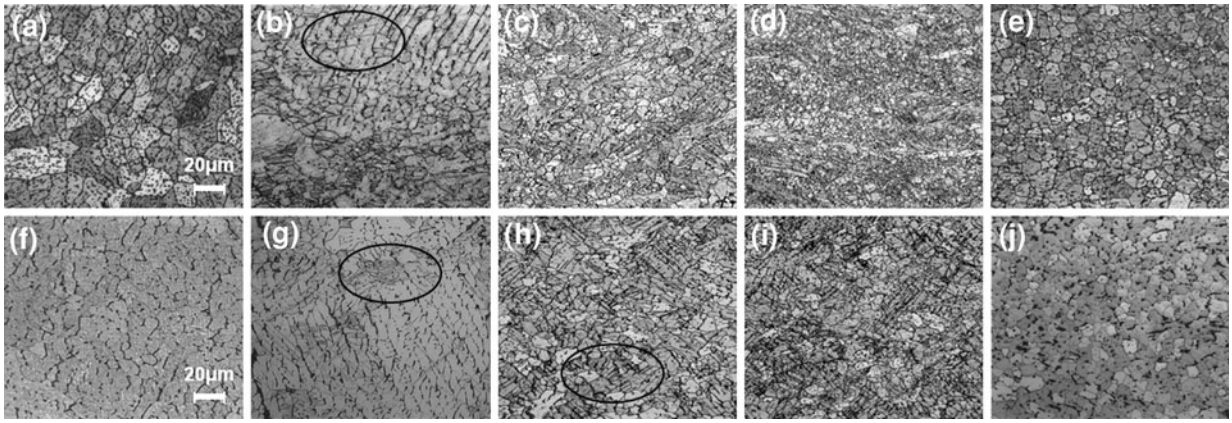

Fig. 2—Optical micrographs of the alloys in various conditions; (*a*) homogenized ZX11, (*b*) 1-pass-rolled ZX11, (*c*) 3-pass-rolled ZX11, (*d*) 5-pass-rolled ZX11, (*e*) annealed ZX11, (*f*) homogenized ZX61, (*g*) 1-pass-rolled ZX61, (*h*) 3-pass-rolled ZX61, (*i*) 5-pass-rolled ZX61, and (*j*) annealed ZX61.

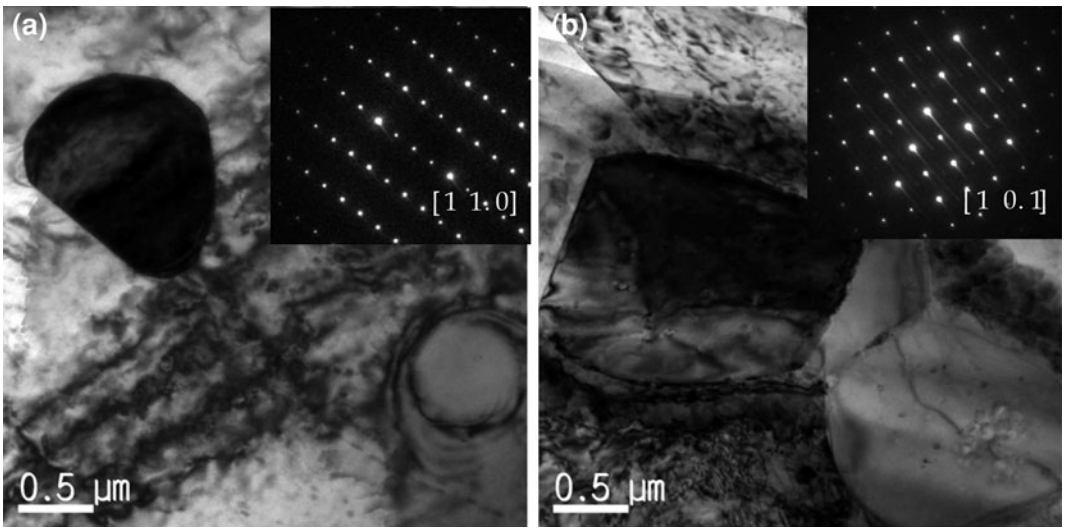

Fig. 3—TEM micrographs of second-phase particles; (*a*) ZX11 and (*b*) ZX61.

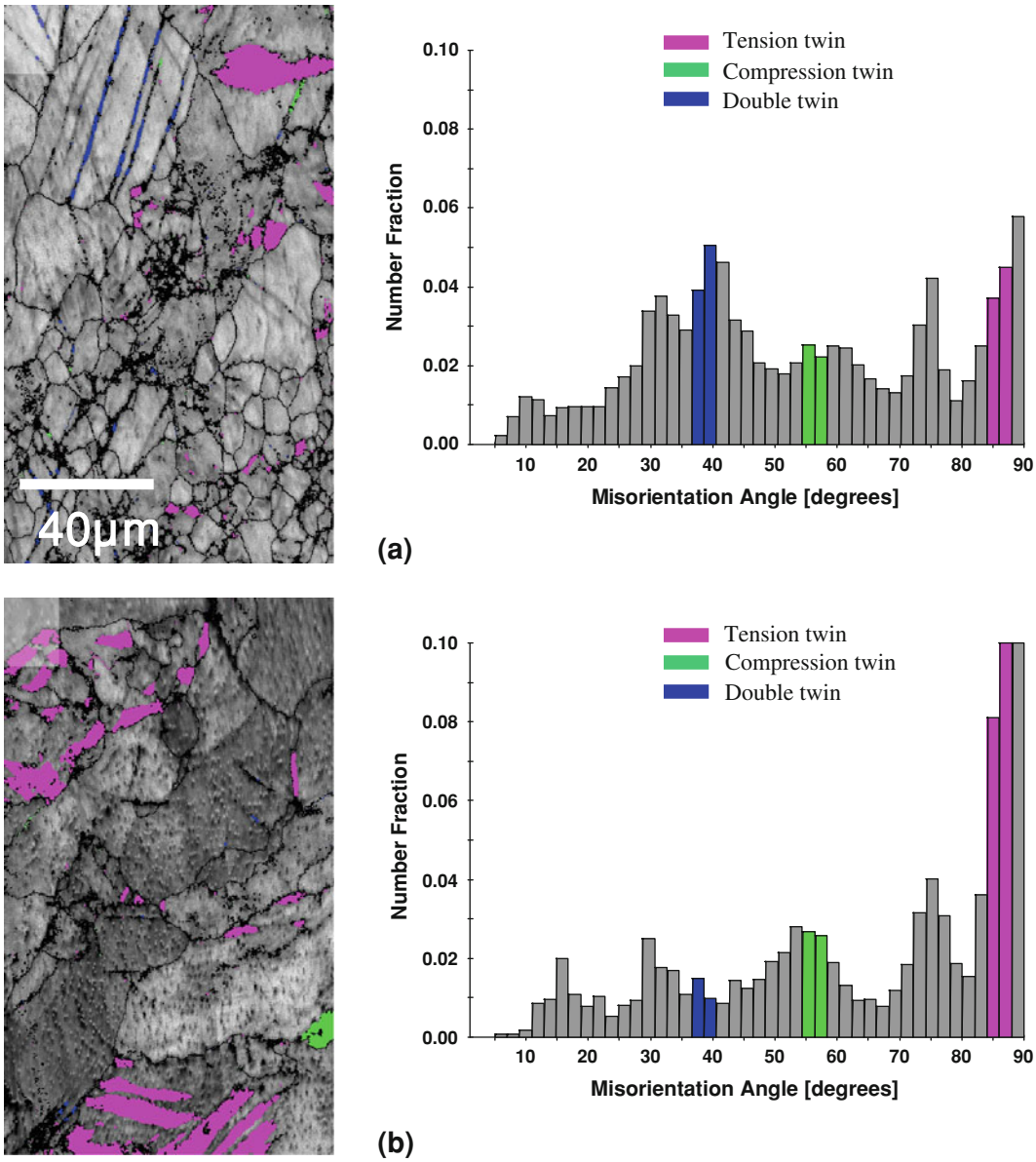

Fig. 4—EBSD image quality maps and boundary misorientation distribution of the alloys in (*a*) 1-pass-rolled ZX11 and (*b*) 1-pass-rolled ZX61. Types of twins are identified in EBSD maps with their respective colors.

both double and tension twins decrease with rolling, tension twins disappear at an earlier stage of rolling than double twins. After the final annealing (Figure 5(e)), the distribution of the misorientation angles becomes similar to that of the as-homogenized sheet (Figure 5(a)). ZX61 shows a quite different distribution of misorientation angles as compared to ZX11. Even in the as-homogenized condition (Figure 5(f)), ZX61 shows a large fraction near the misorientation angle of 86 associated with tension twins, in addition to that of 30 deg, which is commonly observed in textured Mg alloys.[10] Such a large fraction near the misorientation angle of 86 deg is maintained up to the final rolling pass (Figure 5(i)). After the final annealing (Figure 5(j)), the distribution of misorientation angles in ZX61 becomes similar to that in ZX11 (Figure 5(e)), except the slightly larger fraction of misorientation angles near 86 deg in the former than in the latter. The above-mentioned difference in the distribution of misorientation angles between ZX11 and ZX61 would be reflected in the texture profiles as shown below.

B. *Texture Development*

Figure 6 shows the (00.2) pole figures of the alloy sheets in various conditions. It shows that the homogenized ZX11 has a basal texture (Figure 6(a)), typical of Mg alloys, although its maximum intensity is rather low. As shown in Figure 6(b), the first rolling of the homogenized sheet does not result in any significant change in the texture, except the strengthening of basal texture intensity. The maximum intensity of the basal poles decreases upon reheating without any other significant change in the texture. A significant change

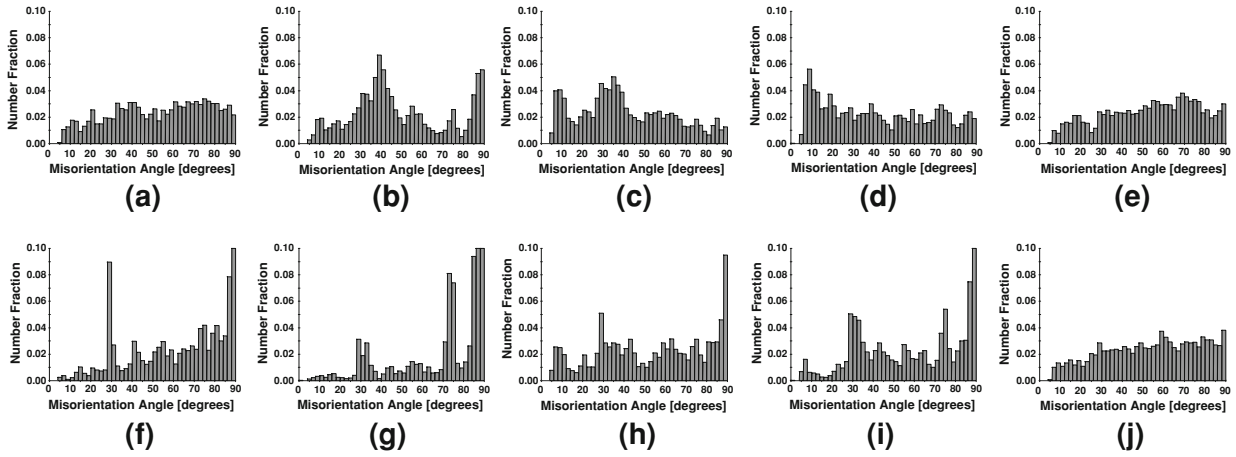

Fig. 5—Boundary misorientation distribution; (*a*) homogenized ZX11, (*b*) 1-pass-rolled ZX11, (*c*) 3-pass-rolled ZX11, (*d*) 5-pass-rolled ZX11, (*e*) annealed ZX11, (*f*) homogenized ZX61, (*g*) 1-pass-rolled ZX61, (*h*) 3-pass-rolled ZX61, (*i*) 5-pass-rolled ZX61, and (*j*) annealed ZX61.

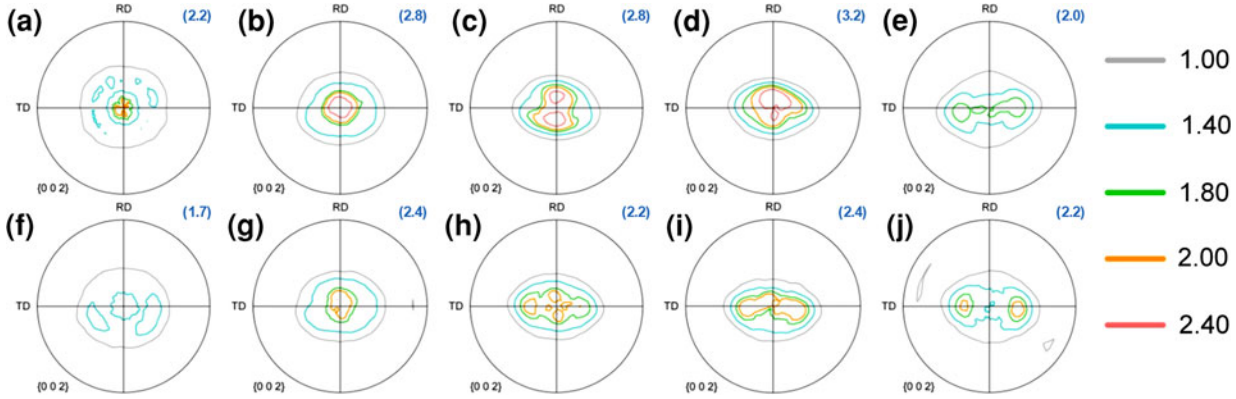

Fig. 6—(00.2) pole figures of the alloys in various conditions; (*a*) homogenized ZX11, (*b*) 1-pass-rolled ZX11, (*c*) 3-pass-rolled ZX11, (*d*) 5-pass-rolled ZX11, (*e*) annealed ZX11, (*f*) homogenized ZX61, (*g*) 1-pass-rolled ZX61, (*h*) 3-pass-rolled ZX61, (*i*) 5-pass-rolled ZX61, and (*j*) annealed ZX61. Number in parenthesis indicates the maximum intensity.

in the texture occurs after subsequent rolling. As can be seen in Figure 6(c), there is a splitting of the basal poles toward the RD, similar to the results found in some RE-containing alloys.[10–13] Such a texture is maintained up to the final rolling pass (fifth pass) with an increase in the maximum intensity (Figure 6(d)). However, a significant change in texture occurs in ZX11 after the final annealing, as shown in Figure 6(e). Besides a large decrease in the maximum intensity after the final annealing, there is a splitting of basal poles toward the TD, which is totally different from the texture of rolled sheets showing the splitting of basal poles toward the RD. As shown in Figures 6(f) through (i), the texture evolution of ZX61 with rolling is different from that of ZX11. ZX61 shows the splitting of basal poles toward the TD even in the as-homogenized condition (Figure 6(f)). After the first rolling pass, the basal poles are somewhat oriented toward the RD (Figure 6(g)), but rotate back to the TD after a subsequent rolling pass (Figure 6(h)). Such a texture is maintained up to the final rolling pass (Figure 6(i)) and after annealing (Figure 6(j)). It can also be seen that the maximum intensity does not change appreciably with the number of rolling passes in the case of ZX61.

As shown above, ZX alloys show a quite different texture as compared to those of conventional Mg alloys including Mg-Zn alloys. Although there is no information available on the effect of Zn content on texture, a comparison of the similar Mg-Zn alloys with different Zn content, ZM21[23] and ZMA611,[16] shows that both alloys show similar texture, suggesting that Zn content does not affect the texture evolution in Mg-Zn alloys. Therefore, the unique texture observed in ZX alloys can be ascribed to the addition of Ca. The most interesting point in texture evolution of ZX11 is that the texture obtained during rolling shows a splitting of basal poles toward the RD, while that after annealing becomes quite different, showing a spitting of basal poles toward the TD. To understand the details of texture evolution, variation in the ODFs with rolling was analyzed.

Figure 7 shows the 0 and 30 deg sections of the ODFs (Bunge-Euler angles)[24] describing textures of the sheets in various conditions. The major texture components present in the alloy sheets are schematically shown in Figures 7(a) and (b), and their locations on (00.2) pole

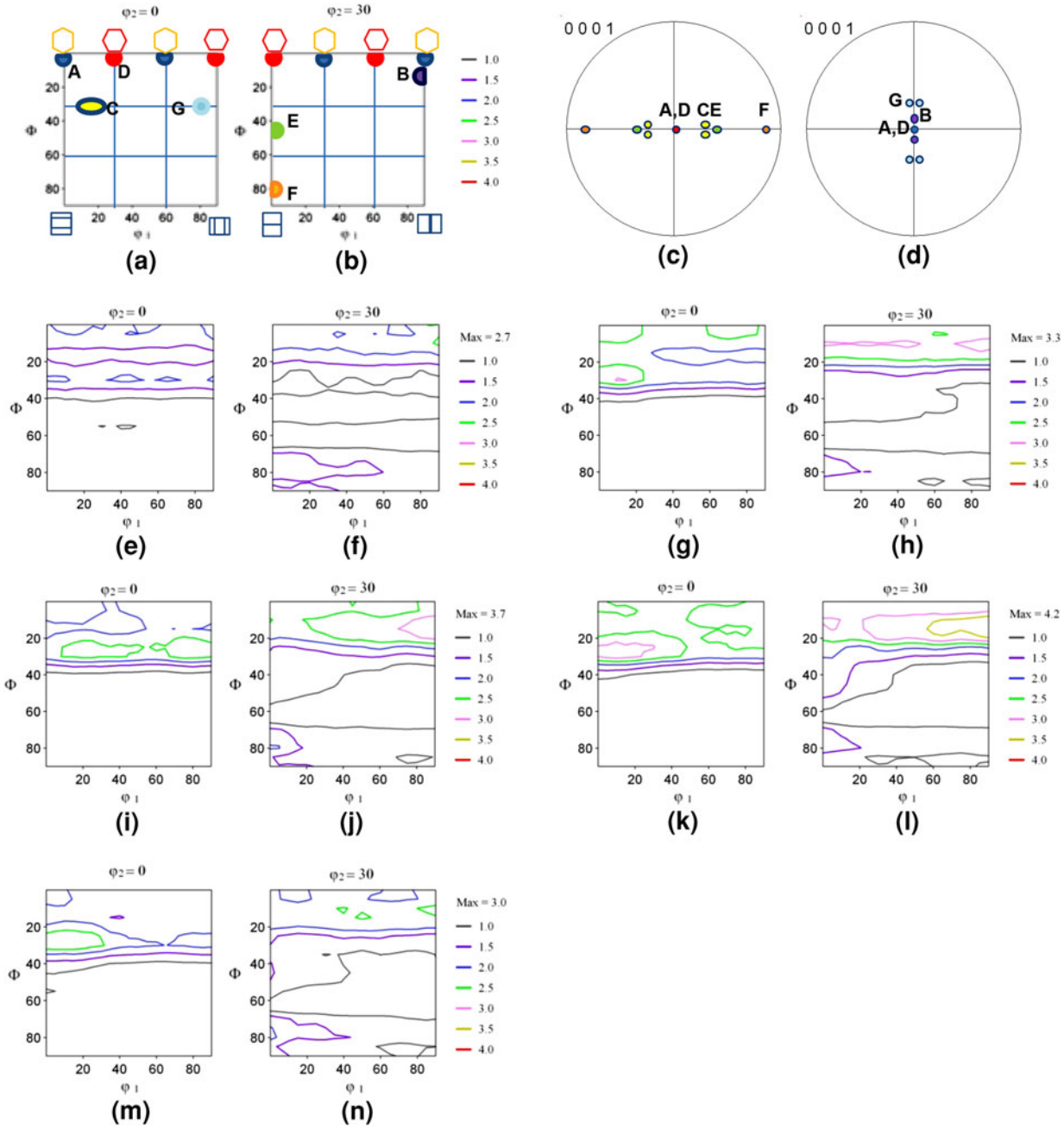

Fig. 7—(*a*, *b*) schematics for the distribution of the major texture components, (*c*, *d*) schematics for the position of the major texture components in (00.2) pole figure, and (*e* through *n*) ODF sections of ZX11 in various conditions for $\varphi_2 = 0^{\circ}$ and $\varphi_2 = 30^{\circ}$. (e, f) homogenized, (g, h) 1-pass-rolled, (i, j) 3-pass-rolled, (k, l) 5-pass-rolled, and (m, n) annealed.

figures are indicated in Figures 7(c) and (d). These components can be characterized as follows: the component A ($\varphi_1 = 0$ deg, $\Phi = 0$ deg, $\varphi_2 = 0$ deg) is characterized as $\{00.1\}\langle 11.0\rangle$; B ($\varphi_1 = 90$ deg, $\Phi = 10$ deg, $\varphi_2 = 30$ deg), $\{00.1\}\langle 11.0\rangle$ tilted at 10 deg from ND to RD; C ($\varphi_1 = 10$ to 20 deg, $\Phi = 30$ deg, $\varphi_2 = 0$ deg), $\{00.1\}\langle 11.0\rangle$ tilted at 30 deg and 10 to 20 deg from ND to TD and TD to RD, respectively; D ($\varphi_1 = 30$ deg, $\Phi = 0$ deg, $\varphi_2 = 0$ deg), $\{00.1\}\langle 10.0\rangle$; E ($\varphi_1 = 0$ deg, $\Phi = 45$ deg, $\varphi_2 = 30$ deg), $\{00.1\}\langle 10.0\rangle$ tilted at 45 deg from ND to TD; F ($\varphi_1 = 0$ deg, $\Phi = 80$ deg, $\varphi_2 = 30$ deg), $\{00.1\}\langle 10.0\rangle$ tilted at 80 deg from ND to TD; and G ($\varphi_1 = 80$ deg, $\Phi = 30$ deg, $\varphi_2 = 0$ deg), $\{00.1\}\langle 11.0\rangle$ tilted at 30 and 80 deg from ND to TD and TD to RD, respectively. Among these, the components A and D represent the components responsible for the basal poles along the ND, the components B and G for the broadening or splitting of the basal poles from the ND to the RD, and the components C, E, and F for the broadening or splitting of the basal poles from the ND to the TD, as schematically shown in Figures 7(c) and (d).

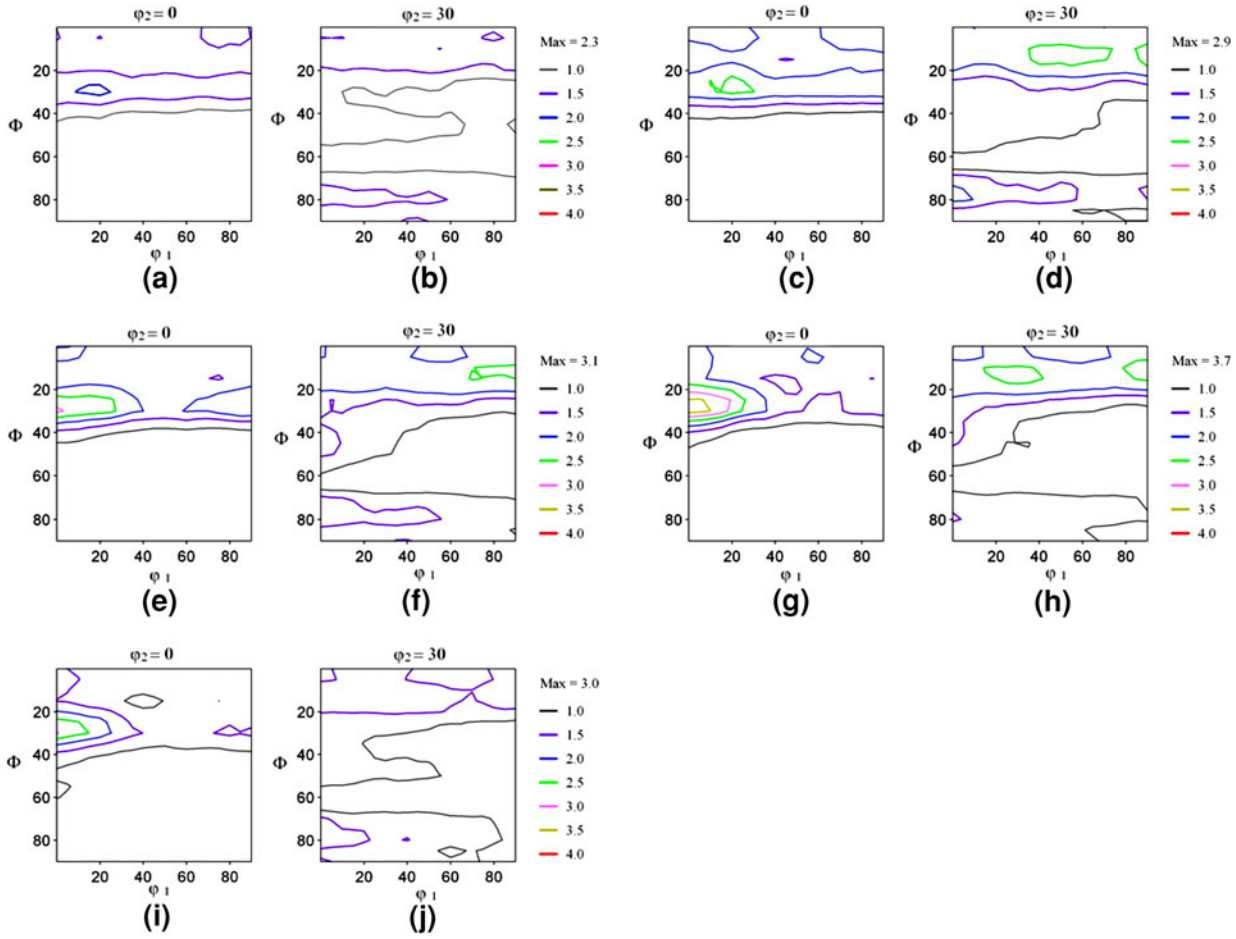

Fig. 8—ODF sections of ZX61 in various conditions for $\varphi_2 = 0$ deg and $\varphi_2 = 30$ deg. (*a*, *b*) homogenized, (*c*, *d*) 1-pass-rolled, (*e*, *f*) 3-pass-rolled, (*g*, *h*) 5-pass-rolled, and (*i*, *j*) annealed.

As can be seen in Figures 7(e) and (f), the texture of the homogenized ZX11 alloy sheet is characterized by the formation of {00.1} fiber texture (A and D components) along with {01.3} fiber texture, including the component C. In addition, there is a development of the component B as well as the scattered component F. Among these components, B is the strongest. Changes in the texture component after the first rolling pass are shown in Figures 7(g) and (h). It shows that all the components except F show increases in intensity. With increase in the number of rolling passes (Figures 7(i) through (l)), the component B shows the largest increase in intensity followed by the component E, while other components do not show an appreciable change in intensity. After final annealing (Figures 7(m) and (n)), all the components except F show decreases in intensity and the strongest component becomes C, followed by the component B.

The texture of the homogenized ZX61 alloy sheet is characterized by {01.3} fiber texture, including the strongest component C (Figures 8(a) and (b)). In addition, there is a development of the second strongest component B as well as the scattered component F along with the components A and D. After the first rolling pass (Figures 8(c) and (d)), all the components except E become stronger as compared to the as-homogenized condition. With an increase in the number of rolling passes (Figures 8(e) through (h)), there is a large increase in intensity of the component C and a small increases for the components B and E, while other components show decreases in the intensity. After the final annealing (Figures 8(i) and (j)), all the components show decreases in intensity and the strongest component becomes C, followed by the component B, similar to the texture of annealed ZX11.

C. *Mechanical Properties*

The tensile properties of the alloys in the annealed condition are shown in Table I. It shows that ZX11 has yield strength of 154.9 MPa, tensile strength of 234.3 MPa, uniform elongation of 11.6 pct, and total elongation of 12.3 pct. ZX61 has better tensile properties than ZX11, with yield strength of 163.6 MPa, tensile strength of 258.9 MPa, uniform elongation of 15.5 pct, and total elongation of 17.2 pct. The elongation values of these alloys are somewhat smaller than expected considering their weak texture. For example, the similarly textured

Table I. Tensile Properties and LDH Values of the Alloys

Alloy	YS (MPa)	UTS (MPa)	E_U (pct)	E_T (pct)	LDH (mm)
ZX11	154.9	234.3	11.6	12.3	8.8
ZX61	163.6	258.9	15.5	17.2	7.5

Mg-1Zn-1Gd alloy shows total elongation of 29 pct with yield strength of 181 MPa,[25] which is much higher than those of ZX alloys. Nevertheless, both alloys show exceptional stretch formability with LDH values of 8.8 and 7.5 mm for ZX11 and ZX61, respectively, exceeding that of 5052 Al alloy having a lower strength level.[1] Yield strength values of these alloys are higher than those of other Mg alloys having similar LDH values.[1,4,26]

IV. DISCUSSION

The texture evolution in Mg alloys is very complex to understand since it involves the formations of deformation texture and dynamic recrystallization texture during the rolling as well as static recrystallization texture during the reheating and final annealing. Since the change in the texture by reheating is not significant except for small decreases in the strength of major components, the following discussion will be on the texture evolution by the rolling and final annealing.

A. *Deformation Texture*

As shown above, the most important texture components for the alloys are B and C. The variations in their intensities with rolling steps are replotted as shown in Figure 9. It can be seen that throughout all stages of rolling, the component B is always stronger than the component C in ZX11, while the component C is always stronger than the component B in ZX61. Such a difference in the activities of the components B and C is reflected in the pole figures (Figure 6), showing the splitting of the basal poles along the RD and TD in rolled ZX11 and ZX61, respectively.

These results clearly suggest that different deformation mechanisms are operating during rolling for different alloys, which might result in differences in the nature of deformation texture between two alloys. As shown in Figure 5, there are differences in the variations in the misorientation angles with rolling between two alloys. ZX11 shows high fractions near the misorientation angles of 38 and 86 deg after the first rolling pass (Figure 5(b)). It also shows that the boundaries with misorientation near 38 deg are more frequent than those near 86 deg, indicating that {10.1}{10.2} double twins are more active than {10.2}⟨10.1⟩ tension twins during the first rolling pass. However, the misorientation angle distribution becomes more random as the number of rolling passes increases as shown in Figures 5(c) and (d). This suggests that the twin–matrix orientation relationship is destroyed due to deformation via slip in both the twin and the matrix in order to accommodate the

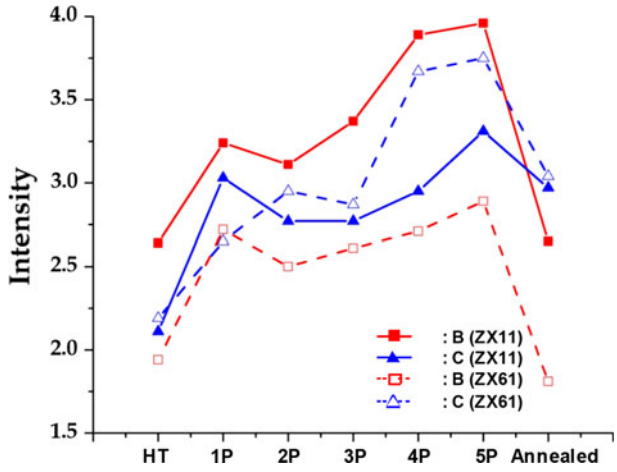

Fig. 9—Variations in the intensities of the major texture components B and C with rolling.

deformation imposed following twin formation.[27] In contrast to ZX11, ZX61 shows the dominance of misorientation near 86 deg at all stages of the rolling steps (Figures 5(g) through (i)), indicating the active formation of tension twins throughout the rolling steps. The misorientation near 38 deg, that for double twins, is not apparent in all cases of ZX61. The reason for the above-mentioned differences in the preference of deformation twins between the two alloys is not clear. A calculation of the phase diagrams for both alloys shows that there is a large difference in the solubility of Ca depending on Zn content. It shows that the solubility of Ca in Mg solid solution at the rolling temperature of 573 K (300 °C) is 0.13 and 0.01 pct for ZX11 and ZX61, respectively. Although there is no available information on the effect of Ca on the critical resolved shear stresses of various twins and dislocations, the present results suggest that Ca reduces the critical resolved shear stress of compression twins considerably, resulting in a more active formation of compression twins and subsequent formation of double twins in ZX11 than ZX61. It has recently been shown that the addition of Y results in the enhanced activity of ⟨c + a⟩ slip and compression and double twinning as compared to pure Mg.[28] Further, it has been shown that based on density functional theory (DFT)-based simulation, the enhanced activation of pyramidal ⟨c + a⟩ dislocations is accompanied by a significant decrease in basal stacking fault energy (SFE) through the addition of Y.[29] Although no calculation was conducted on SFE of other planes and no relationship made between SFE and activities of compression and double twinning, it can be expected that such a decrease in SFE by Y addition would facilitate the activation of compression and double twinning since nucleation of twin involves the formation of partial dislocation and twinning dislocations. This is supported by the report showing that the dissociation of ⟨a⟩, ⟨a + c⟩, or ⟨c⟩ dislocations leads to the generation of twinning dislocations on their respective twin planes.[30] Muzyk *et al.*[31] also reported that the additions of Y, Zr, Zn, Ti, or Al are expected to increase the tendency for mechanical twinning, although their effects on specific

twinning systems are not known. Further studies are certainly needed to clarify the effect of Ca on critical resolved shear stresses of various twins and dislocations either by studies on single crystals or by computer simulation.

The above-mentioned differences in the deformation modes between ZX11 and ZX61 might be reflected in the deformation texture of rolled sheets if there is no significant change in the texture by reheating between rolling passes. ZX11 shows the splitting of basal poles toward the RD, while ZX61 shows the splitting of basal poles toward the TD (Figure 6). There have been several reports showing the splitting of basal poles toward the RD.[10,16,32–34] It has been suggested that the operation of ⟨c + a⟩ slip would rotate the basal poles from the ND toward the RD.[32–34] It has also been suggested that the formation of double twins in deformation bands can induce the splitting of basal poles toward the RD,[16] which agrees with the present results of ZX11. Hantzsche *et al.*[10] reported that deformation bands consisted of compression and double twins in the as-rolled Mg-0.04Nd (at. pct) alloy, showing the splitting of basal poles toward the RD. Although not discussed by the authors, a correlation of texture and deformation twins formed during rolling[10] indicates that compression twins or double twins in deformation bands can also induce the splitting of basal poles toward the RD.

The role of tension twinning in the reorientation of grains during rolling is somewhat controversial. It has been claimed by several researchers that the operation of tension twinning during deformation is one of main factors responsible for the formation of a basal-type texture in Mg alloys.[35] On the other hand, a consideration of Schmid factors for the selection and formation of tension twins during the rolling of initially randomly oriented alloys shows that tension twinning leads to the broadening of basal poles from the ND toward the TD,[16] which supports the present observation of splitting of basal poles toward the TD in ZX61 having a large amount of tension twins. The activation of prismatic ⟨a⟩ slip has also been suggested to be responsible for the splitting of basal poles toward the TD.[4,26]

B. *Annealing Texture*

As mentioned previously, the most striking change induced by the final annealing is the rotation of basal poles from the RD to the TD in ZX11 along with a large decrease in maximum intensity, while there is no significant change in texture except a small decrease in maximum intensity in the case of ZX61, which already shows a splitting of basal poles toward the TD in the as-rolled condition. Although there have been numerous studies on the development of recrystallization texture in Mg alloys, the detailed mechanisms are not clear yet. There are several mechanisms proposed for the texture development of Mg alloys by recrystallization: (a) particle-stimulated nucleation (PSN) of recrystallization,[36] (b) recrystallization at deformation or shear bands,[10,16] and (c) change in grain boundary mobility by solutes or second-phase particles.[18,37–39] The present alloys all contain second-phase particles and it might be expected that the recrystallization texture would be modified by the PSN mechanism. Detailed microstructural analyses show that there is indeed the formation of fine recrystallized grains along second-phase particles in annealed alloys as shown in Figure 10. The orientation of PSN-induced recrystallized grains is random as shown in Figure 10(d), similar to an observation made by Robson *et al.*[40] However, the conclusive relationship between such PSN-induced recrystallization and the texture observed in the alloys has not been found. This might be due to the lesser effectiveness of PSN as compared to other recrystallization mechanisms as pointed out by Robson *et al.*[40] Moreover, the PSN of recrystallization would not lead to the splitting of basal poles toward the TD or RD observed in the present study.

On the other hand, the texture evolution in ZX alloys by annealing can be thought as a result of combined effects of recrystallization at deformation bands and preferential growth of non-basal grains due to a change in grain boundary mobility by solutes or second-phase particles. When there is not much difference between the deformation texture and recrystallization texture such as the case of ZX61, it is often hypothesized that all the nuclei are formed during hot rolling and these original nuclei eventually consume the microstructure during recrystallization, *i.e.*, an oriented-nucleation controlled rather than an orientation-growth controlled.[39] In such a case, growth of nuclei during annealing would not significantly affect the texture. Such oriented-nucleation controlled recrystallization has been reported in previous studies on AZ31, which show that recrystallization or grain growth during annealing does not significantly change the texture present in the as-rolled condition.[37,39] Similar behavior has also been observed in RE-containing alloys.[10,16,42] Despite the similarity in the texture between the ZX61 sheets subjected to the fifth rolling pass (Figure 6(i)) and the annealing (Figure 6(j)), the distribution of the boundary misorientation angle becomes much more random after annealing as shown in Figures 5(i) and (j). It is suggested that such a change in the distribution of misorientation angle by annealing could be due to the more favored movement of tension twin boundaries over other boundaries during annealing. Figure 11 shows the microstructures of the three-pass-rolled alloy before and after annealing at 713 K (440 °C) for 40 seconds. It shows that with annealing tension, twins grow consuming the neighboring matrix grains (Figures 11(a) and (b)), while double twins are consumed by the growth of neighboring matrix grains (Figures 11(c) and (d)). It is known that tension twin has a great mobility due to the small mismatch and large step height of the twin boundary.[43] On the other hand, it has been recently suggested that grain boundary mobility of RE-containing Mg alloys could be reduced due to Zener drag induced by the presence of second-phase particles along grain boundaries[38] or solute drag induced by solute segregation along grain boundaries.[37] It has also been reported that Mg-Zn-Ce alloy develops a TD-oriented texture since non-basal orientations develop a form of

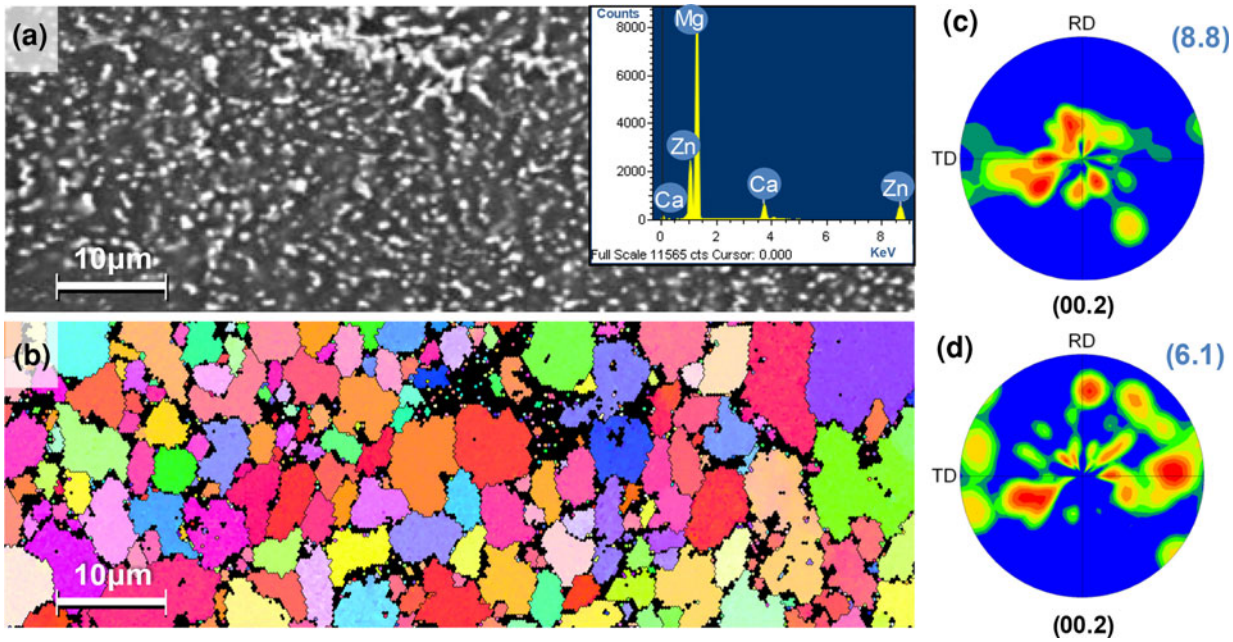

Fig. 10—Microstructure and texture of 3-pass-rolled ZX61 alloy after annealing at 573 K (300 °C) for 50 s; (*a*) SEM image showing the distribution of second-phase particles (inset: EDS spectra from second-phase particles), (*b*) inverse pole figure map, (*c*) (00.2) pole figure before annealing, and (*d*) (00.2) pole figure after annealing.

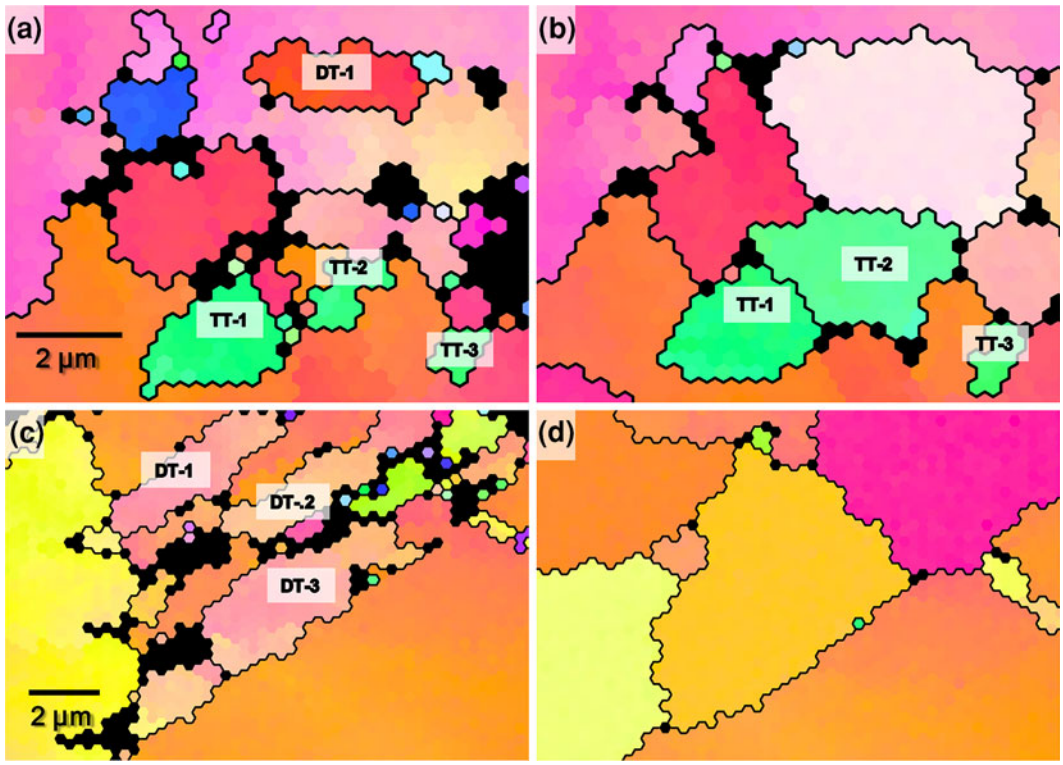

Fig. 11—EBSD inverse pole figure maps of 3-pass-rolled ZX11 alloy; (*a*, *c*) before and (*b*, *d*) after annealing at 713 K (440 °C) for 40 s.

growth advantage, possibly due to a form of particle pinning or solute drag that alters the orientation relationship for high boundary mobility.[41] When the tension twin-oriented grains grow at the expense of neighboring matrix grains such as observed in the present case (Figures 10(a) and (b)), the fraction of the boundary having a misorientation angle near 86 deg associated with tension twins decreases as shown in Figure 5(j). The same argument can be applied to explain a sudden change in the texture of ZX11 by

annealing. The texture of ZX11 is quite different between the as-rolled and as-annealed conditions: a splitting of basal poles toward the RD in the as-rolled condition and a splitting of basal poles toward the TD in the as-annealed condition. The texture of the annealed ZX11 is quite similar to that of the annealed ZX61, suggesting that the nuclei for recrystallization in ZX11 have the same character, *i.e.*, tension twin oriented, as those in ZX61. It appears that ZX11 shows sluggish recrystallization kinetics similar to the results on RE-containing Mg alloys.[35,37,42] In such a case, the nuclei formed during rolling would not have enough driving force to grow during rolling and reheating. The growth of those tension twin-oriented nuclei will occur when the temperature increases, as has been shown in the texture of annealed ZX11 (Figure 6(e)), which was annealed at 713 K (440 °C) much higher than the temperature of rolling and reheating [573 K (300 °C)]. It is also evidenced in the change in the strength of the components B and C, showing that the component C becomes stronger than the component B after annealing (Figure 9). Considering a rather large amount of double twins initially present in rolled ZX11, it is interesting to note that double twins do not grow during annealing as shown in Figures 11(c) and (d), otherwise leading to the splitting of basal poles toward the RD. Similar behavior has been found during static recrystallization of AZ31 alloy,[44] which shows that the growth of new grains from compression and double twins into the matrix is difficult.

As shown above, the texture evolution of ZX11 and ZX61 during rolling and annealing can be explained by considering the operation of deformation twinning (double for ZX11 and tension for ZX61) during the rolling and growth of tension twins for both alloys during annealing. Nevertheless, it is quite possible for pyramidal $\langle c + a \rangle$, prismatic $\langle a \rangle$, and even prismatic $\langle c \rangle$ slips to occur during rolling of these Ca-containing Mg alloys, as observed in several RE-containing alloys. Understanding the effects of these additional slip modes on texture evolution is not an easy task, but is certainly needed to develop Mg alloys with random texture.

C. *Stretch Formability*

The above-mentioned modification of texture by Ca addition to Mg-Zn alloys is certainly beneficial for stretch formability. However, the work-hardening capacities (inverse of yield ratio)[1] of these alloys are rather low: 1.5 for ZX11 and 1.6 for ZX61. Comparing with the LDH values of other alloys at a similar work-hardening capacity, shown in Figure 1 of the reference 1, the LDH values of these ZX alloys are much higher than expected. This suggests that some other deformation mode which does not contribute to work hardening in the uniaxial tensile test is operating during stretch forming. A preliminary study shows that there is an active formation of tension twins during longitudinal tensile straining of both ZX11 and ZX61 alloys, although the stress state is unfavorable for such formation due to the alloys' characteristic texture showing a broadening of angular distribution of basal poles along the TD. Tension twinning in these alloys is believed to be a result of the operation of compressive stress along the TD due to Poisson effect, which is similar to the result found in the Mg-4Zn-1Gd alloy sheet.[45] Such an operation of compressive stress is not possible under the bi-axial stress state experienced during stretch forming, preventing the formation of tension twins. However, a preliminary study on the sheet subjected to stretch forming shows that there is an active formation of tension twins. A detailed investigation on this unusual behavior is underway and will be reported later.

V. SUMMARY

The effect of Ca addition on the texture evolution of ZX11 and ZX61 during rolling and annealing has been investigated and the major findings are summarized as follows:

1. The rolled ZX11 shows a texture having a splitting of basal poles toward the rolling direction, while the rolled ZX61 shows a texture having a splitting of basal poles toward the transverse direction. Such a difference in the deformation texture between two alloys is ascribed to the different type of twins formed during rolling: double twins for ZX11 and tension twins for ZX61.
2. Upon annealing, there is a sudden change in texture of ZX11. The texture having a splitting of basal poles toward the rolling direction in the rolled alloy is replaced by a new texture having a splitting of basal poles toward the transverse direction in the annealed alloy. On the other hand, no significant change in the texture is found in ZX61 after annealing except a slight texture weakening.
3. The characteristic texture of both ZX11 and ZX61 in the annealed condition is ascribed to the preferred growth of tension twin-oriented nuclei during recrystallization.
4. Both ZX11 and ZX61 show an exceptional combination of yield strength and stretch formability.

ACKNOWLEDGMENTS

This work was supported by the WPM Program funded by the Ministry of Industry, Trade and Energy, Korea.

REFERENCES

1. D.H. Kang, D.-W. Kim, S. Kim, G.T. Bae, K.-H. Kim, and N.J. Kim: *Scripta Mater.*, 2009, vol. 61, pp. 768–71.
2. Y. Chino, K. Sassa, and M. Mabuchi: *Mater. Trans.*, 2008, vol. 49, pp. 2916–18.
3. Y. Chino, K. Sassa, and M. Mabuchi: *Mater. Sci. Eng. A*, 2009, vols. 513–514, pp. 394–400.
4. Y. Chino, T. Ueda, Y. Otomatsu, K. Sassa, X. Huang, K. Suzuki, and M. Mabuchi: *Mater. Trans.*, 2011, vol. 52, pp. 1477–82.
5. B. Shin, H. Kang, and D. Bae: *Met. Mater. Int.*, 2012, vol. 18, pp. 23–27.
6. Y. Chino and M. Mabuchi: *Scripta Mater.*, 2009, vol. 60, pp. 447–50.

7. X. Huang, K. Suzuki, and N. Saito: *Scripta Mater*., 2009, vol. 60, pp. 651–54.
8. B. Zhang, Y. Wang, L. Geng, and C. Lu: *Mater. Sci. Eng. A*, 2012, vol. 539, pp. 56–60.
9. X. Huang, K. Suzuki, A. Watazu, I. Shigematsu, and N. Saito: *J. Alloys Compd*., 2009, vol. 470, pp. 263–68.
10. K. Hantzsche, J. Bohlen, J. Wendt, K.U. Kainer, S.B. Yi, and D. Letzig: *Scripta Mater*., 2010, vol. 63, pp. 725–30.
11. S. Sandlöbes, S. Zaefferer, I. Schestakow, S. Yi, and R. Gonzalez-Martinez: *Acta Mater*., 2011, vol. 59, pp. 429–39.
12. M. Sanjari, S.F. Farzadfar, T. Sakai, H. Utsunomiya, E. Essadiqi, I.-H. Jung, and S. Yue: *Mater. Sci. Eng. A*, 2013, vol. 561, pp. 191–202.
13. B.Q. Shi, R.S. Chen, and W. Ke: *Mater. Sci. Eng. A*, 2013, vol. 560, pp. 62–70.
14. Y. Chino, X. Huang, K. Suzuki, K. Sassa, and M. Mabuchi: *Mater. Sci. Eng. A*, 2010, vol. 528, pp. 566–72.
15. T. Al-Samman and X. Li: *Mater. Sci. Eng. A*, 2011, vol. 528, pp. 3809–22.
16. K.-H. Kim, B.-C. Suh, J.H. Bae, M.-S. Shim, S. Kim, and N.J. Kim: *Scripta Mat*., 2010, vol. 63, pp. 716–20.
17. G.T. Bae, J.H. Bae, D.H. Kang, H. Lee, and N.J. Kim: *Met. Mater. Int*., 2009, vol. 15, pp. 1–5.
18. N. Stanford: *Mater. Sci. Eng. A*, 2010, vol. 528, pp. 314–22.
19. C.L. Mendis, J.H. Bae, N.J. Kim, and K. Hono: *Scripta Mater*., 2011, vol. 64, pp. 335–38.
20. S.S. Park, Y.S. Park, and N.J. Kim: *Met. Mater. Int*., 2002, vol. 8, pp. 551–54.
21. S.S. Park, G.T. Bae, D.H. Kang, I.-H. Jung, K.S. Shin, and N.J. Kim: *Scripta Mater*., 2007, vol. 57, pp. 793–96.
22. S.S. Park, W.-J. Park, C.H. Kim, B.S. You, and N.J. Kim: *JOM*, 2009, vol. 61, pp. 14–18.
23. J. Bohlen, M.R. Nürnberg, J.W. Senn, D. Letzig, and S.R. Agnew: *Acta Mater*., 2007, vol. 55, pp. 2101–12.
24. H.J. Bunge and W.T. Roberts: *J. Appl. Crystallogr*., 1969, vol. 2, pp. 116–28.
25. H. Yan, R.S. Chen, and E.H. Han: *Mater. Sci. Eng. A*, 2010, vol. 527, pp. 3317–22.
26. D. Wu, R.S. Chen, and E.H. Han: *J. Alloys Compd*., 2011, vol. 509, pp. 2856–63.
27. Y.B. Chun, S.H. Yu, S.L. Semiatin, and S.K. Hwang: *Mater. Sci. Eng. A*, 2005, vol. 398, pp. 209–19.
28. S. Sandlöbes, S. Zaefferer, I. Schestakow, S. Yi, and R. Gonzalez-Martinez: *Acta Mater*., 2012, vol. 59, pp. 429–39.
29. S. Sandlöbes, M. Friák, S. Zaefferer, A. Dick, S. Yi, D. Letzig, Z. Pei, L.F. Zhu, J. Neugebauer, and D. Raabe: *Acta Mater*., 2012, vol. 60, pp. 3011–21.
30. S. Mendelson: *J. Appl. Phys*., 1970, vol. 41, pp. 1893–1910.
31. M. Muzyk, Z. Pakiela, and K.J. Kurzydlowski: *Scripta Mater*., 2012, vol. 66, pp. 219–22.
32. R. Cottam, J. Robson, G. Lorimer, and B. Davis: *Mater. Sci. Eng. A*, 2008, vol. 485, pp. 375–82.
33. S.R. Agnew, M.H. Yoo, and C.N. Tome: *Acta Mater.,* 2001, vol. 49, pp. 4277–89.
34. A. Styczynski, C. Hartig, J. Bohlen, and D. Letzig: *Scripta Mater*., 2004, vol. 50, pp. 943–47.
35. D.W. Brown, S.R. Agnew, M.A.M. Bourke, T.M. Holden, S.C. Vogel, and C.N. Tome: *Mater. Sci. Eng. A*, 2005, vol. 399, pp. 1–12.
36. L.W.F. Mackenzie, B. Davis, F.J. Humphreys, and G.W. Lorimer: *Mater. Sci. Technol*., 2007, vol. 23 (10), pp. 1173–80.
37. J.P. Hadorn, K. Hantzsche, S. Yi, J. Bohlen, D. Letzig, J.A. Wollmershauser, and S.R. Agnew: *Metall. Mater. Trans. A*, 2012, vol. 43A, pp. 1347–62.
38. J.P. Hadorn, K. Hantzsche, S. Yi, J. Bohlen, D. Letzig, J.A. Wollmershauser, and S.R. Agnew: *Metall. Mater. Trans. A*, 2012, vol. 43A, pp. 1363–75.
39. Y.B. Chun, J. Geng, N. Stanford, C.H.J. Davies, J.F. Nie, and M.R. Barnett: *Mater. Sci. Eng. A*, 2011, vol. 528, pp. 3653–58.
40. J.D. Robson, D.T. Henry, and B. Davis: *Acta Mater*., 2009, vol. 57, pp. 2739–47.
41. L.W.F. Mackenzie and M. Pekguleryuz: *Mater. Sci. Eng. A*, 2008, vol. 480, pp. 189–97.
42. S.A. Farzadfara, M. Sanjaria, I.-H. Jung, E. Essadiqi, and S. Yue: *Mater. Sci. Eng. A*, 2011, vol. 528, pp. 6742–53.
43. J.F. Bingert, T.A. Mason, G.C. Kaschner, P.J. Maudlin, and G.T. Gray, III: *Metall. Mater. Trans. A*, 2002, vol. 33A, pp. 955–65.
44. X. Li, P. Yang, L.-N. Wang, L. Meng, and F. Cui: *Mat. Sci. Eng. A*, 2009, vol. 517, pp. 160–69.
45. B.-C. Suh, M.-S. Shim, D.-W. Kim, and N.J. Kim: unpublished research, 2013.